



Experimental study on the influence of the angle of attack on cavity evolution and surface load in the water entry of a cylinder

Tiezhi Sun ^{a,b}, Chongbin Shi ^a, Guiyong Zhang ^{a,b,c,*}, Zhi Zong ^{a,b,c}, Heng Wang ^a

^a School of Naval Architecture, Dalian University of Technology, Dalian, 116024, China

^b State Key Laboratory of Structural Analysis for Industrial Equipment, Dalian University of Technology, Dalian, 116024, China

^c Collaborative Innovation Center for Advanced Ship and Deep-Sea Exploration, Shanghai, 200240, China

ARTICLE INFO

Keywords:

Water entry
Angle of attack
Cavity evolution
Load characteristics

ABSTRACT

The characteristics of cavity evolution and surface load in water entry by a constrained-posture cylinder at different angles of attack are experimentally investigated. High-speed photography is used to capture flow behaviors, and a measurement system is established to measure the pressure on the surface of the cylinder and its acceleration during the process of water entry. The experimental results show that when the cylinder enters the water at a certain angle of attack, the cavity shows an obvious asymmetry. Comparison of angles of attack shows that the cavity evolution and load characteristics during the water entry process are closely related to the angle of attack of the cylinder. Increasing the angle of attack can shorten the period of cavity pinch-off but prolong the time of surface seal. Meanwhile, the peak value of impact pressure shows a gradual downward trend with the increased angle of attack, and the relationship between the duration of high load and the angle of attack is approximately linear. Moreover, the characteristics of the flow field play an important role in the surface load of the cylinder, an obvious and short-lived negative relative pressure will appear on the surface of the model inside the cavity at the initial stage of water entry, the part of cylinder that is not affected by the cavity and directly interacts with water has a continuous positive pressure trend. In addition, it can be found that there is a significant pressure fluctuation when the cavity separation line passes over the surface.

1. Introduction

The problem of water entry is typically encountered in ocean engineering, and it has a wide range of military and civilian applications, such as in air-dropped torpedoes, rocket booster recovery, aircraft landing on water surfaces, and hull slamming due to waves. Water entry is a multiphase flow process with transient and nonlinear flow. Due to the sudden change in medium at the moment of impact, a great impact load appears on the part that contacts the water, which may cause deformation and damage and lead to a failure of internal components, resulting in serious adverse effects. The problem of cavity evolution and the load characteristics of water entry has received widespread attention from researchers.

The theoretical study of water entry began in the 1920s. Von Karman (1929) put forward the concept of additional mass, extrapolated from the law of conservation of momentum, and thus obtained a theoretical method of solving the impact load of a two-dimensional wedge during water entry. On this basis, Wagner (1932) addressed pressure

distribution on the surface of the wedge, which laid a foundation for later theoretical research. However, Wagner's model did not consider air cushion effects. Verhagen (1967) incorporated the phenomenon of air cushion combined with the air compressibility and presented a model of pressure prediction. Lee et al. (1997), drawing on the principle of the conservation of energy, studied cavity evolution and established a dynamic model of the cavity in relation to a projectile in high-speed water entry. Duez et al. (2007) proposed a relationship between the critical speed of the formation of the water entry cavity and the contact angle with the surface. The critical speed changes little with the contact angle for angles less than 90°. Xu et al. (2008) analyzed the oblique water entry of an asymmetrical wedge based on the complex velocity potential using the boundary element method. In particular, it was encouraging to observe the sharp variation and negative pressure near the tip of the wedge. Ding et al. (2015), using the Rayleigh–Besant equation, established the cavity dynamic model to accurately obtain the characteristics of the radial expansion of the cavity.

Due to imperfections in the theoretical approach, experimental

* Corresponding author. School of Naval Architecture, Dalian University of Technology, Dalian, 116024, China.

E-mail address: gzhang@dlut.edu.cn (G. Zhang).

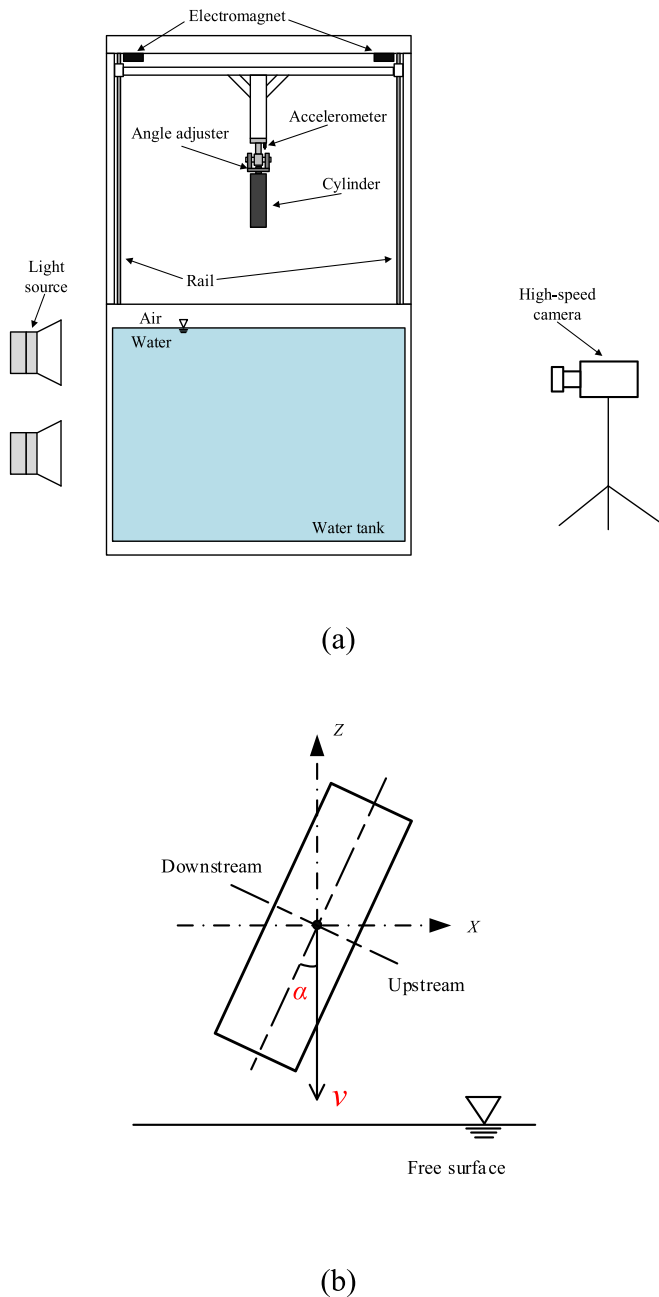


Fig. 1. Schematic of the experimental setup and the state of water entry: (a) main test system and (b) definition of initial parameters of water entry.

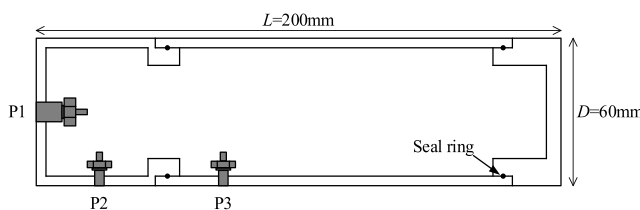
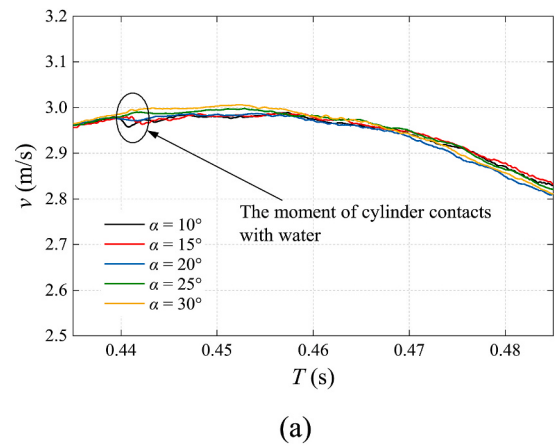
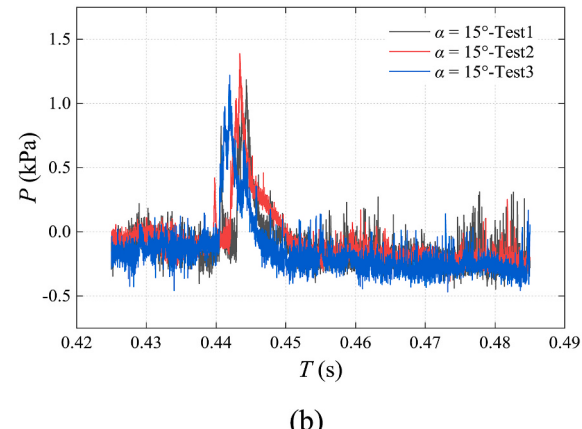


Fig. 2. Schematic of the internal layout of the cylinder.

research on the water entry problem developed only gradually. Since the beginning of the 20th century, study of water entry has been conducted using high-speed photography. [Worthington and Cole \(1897\)](#) used this



(a)



(b)

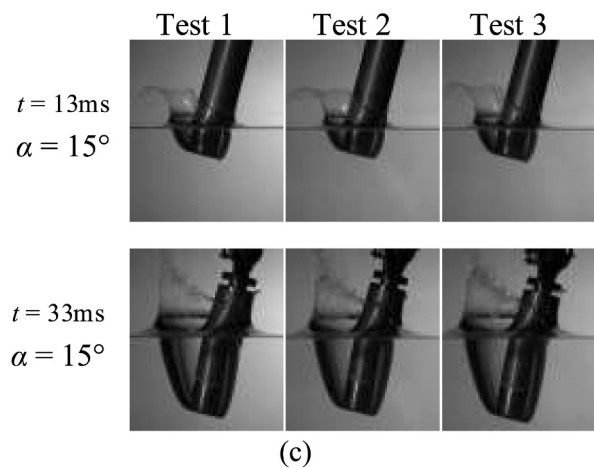


Fig. 3. Repeatability test by (a) Velocity curve of the cylinder (b) pressure curves of P2 (c) cavity splash.

means to capture the typical characteristics of the vertical water entry of spheres, such as cavity, splash, and surface seal, and this led to further developments in the understanding of the phenomenon. Due to the sphere's radial symmetry, it offers certain advantages for research in mechanics, so early work on water entry centered on spheres. [Bell \(1924\)](#) showed the effects of surface tension, viscosity, and surface layers on the impact of a solid sphere on a fluid surface. [Gilberg and](#)

Table 1

Experimental conditions.

Parameter	Symbol	Range/value	Unit
Diameter	D	60	mm
Length	L	200	mm
Mass	m_c	1.25	kg
Initial velocity	v_0	2.96–3.01	m/s
Attack angle	α	10–30	°

Anderson (1948) conducted experimental study on the water entry of a sphere under different types of environmental pressure, and their results showed that environmental pressure could affect the characteristics of splash and cavity evolution in water entry. May and Woodhull (1948) and May (1951; 1952) carried out a series of experiments with spheres having different parameters and analyzed the influence of initial conditions on the cavity and resistance coefficient. Richardson (1948) conducted a series of studies on the vertical and inclined water entry of a rotating body. He analyzed the hydrodynamic characteristics of the

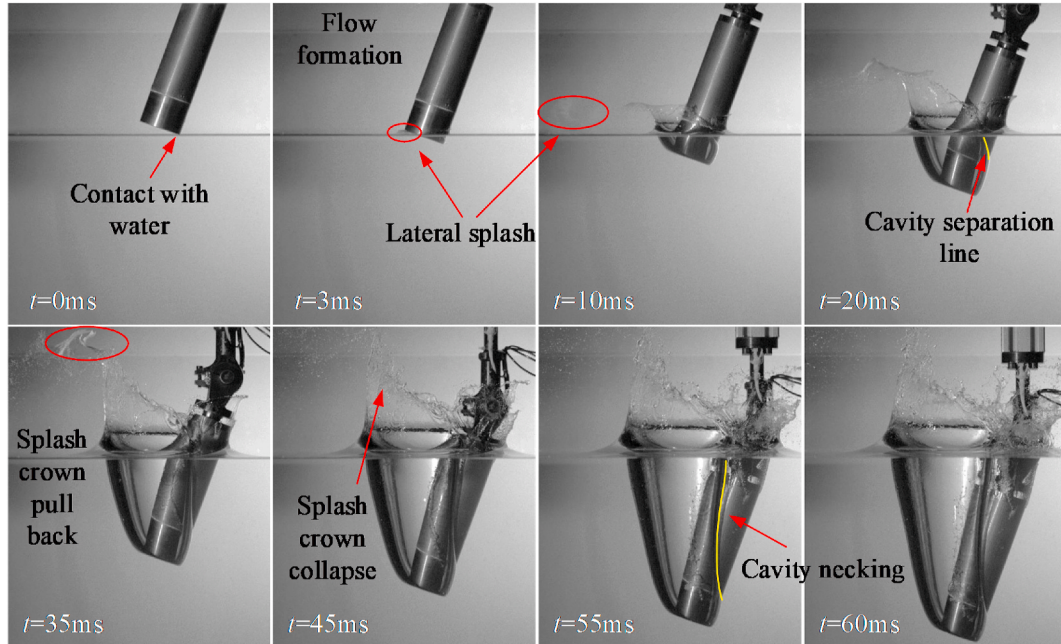
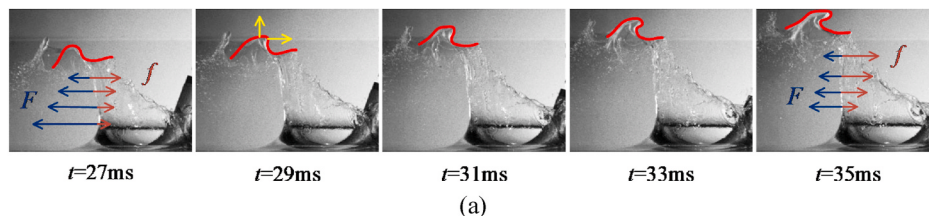
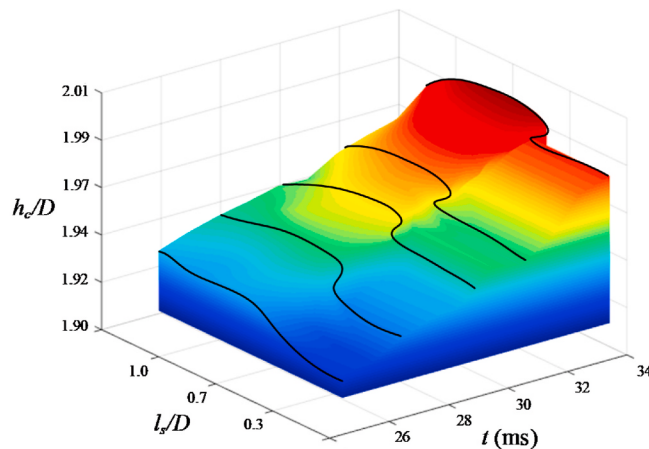


Fig. 4. The evolution of the cavity.



(a)



(b)

Fig. 5. Schematic of the splash crown phenomenon: (a) characteristics of sufferance force and (b) outline of the top of splash crown ($t = 25$ – 35 ms).

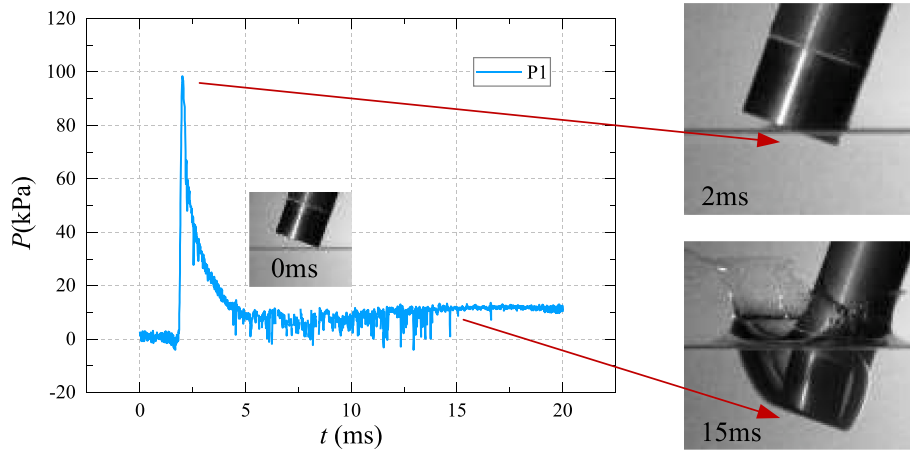


Fig. 6. Pressure versus time curves for P1 ($\alpha = 20^\circ$, $v_0 = 2.99$ m/s).

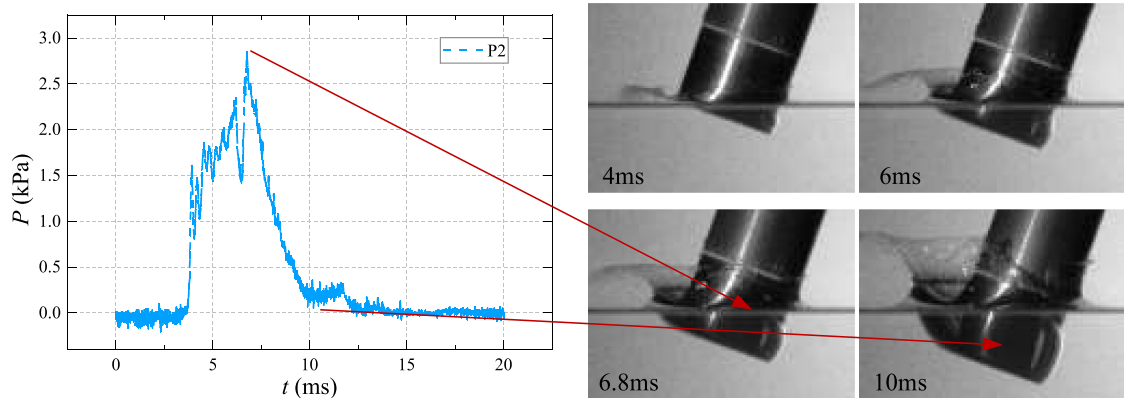


Fig. 7. Pressure versus time curves for P2 ($\alpha = 20^\circ$, $v_0 = 2.99$ m/s).

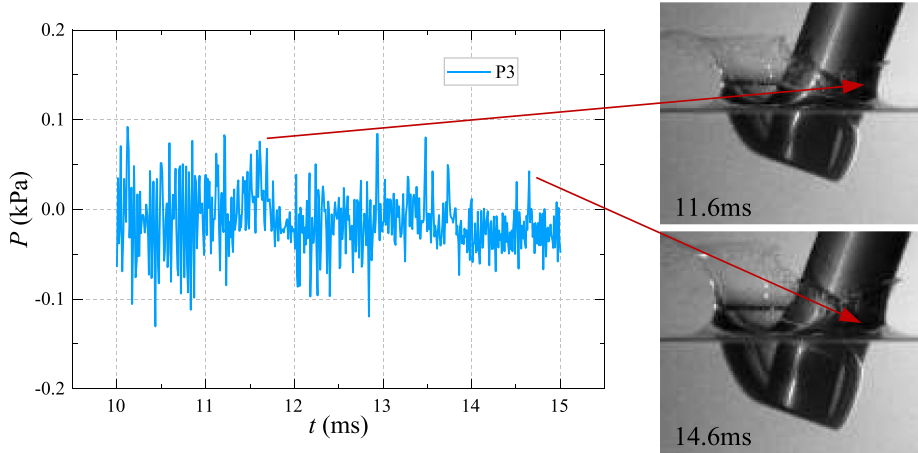


Fig. 8. Pressure versus time curves for P3 ($\alpha = 20^\circ$, $v_0 = 2.99$ m/s).

entry and discussed the bounce phenomenon during entry. Greenhow (1987) studied the two-dimensional entry of wedges of various angles into initially calm water based on theoretical approaches. Excellent results of free surface displacements and pressure distributions on the wetted wedge surface were obtained. Aristoff et al. (2008; 2009) carried out a series of experiments on the water entry of hydrophobic spheres.

Particular attention was paid to the shape of the resulting air cavity in the low Bond numbers. Truscott and Techet (2009) studied the hydrodynamic characteristics of the water entry of a spinning sphere at low Froude numbers and described the phenomenon of splash seal and cavity pinch-off. Hurd et al. (2017) focused on the characteristics of the water entry of deformable elastomeric spheres and found that the cavity

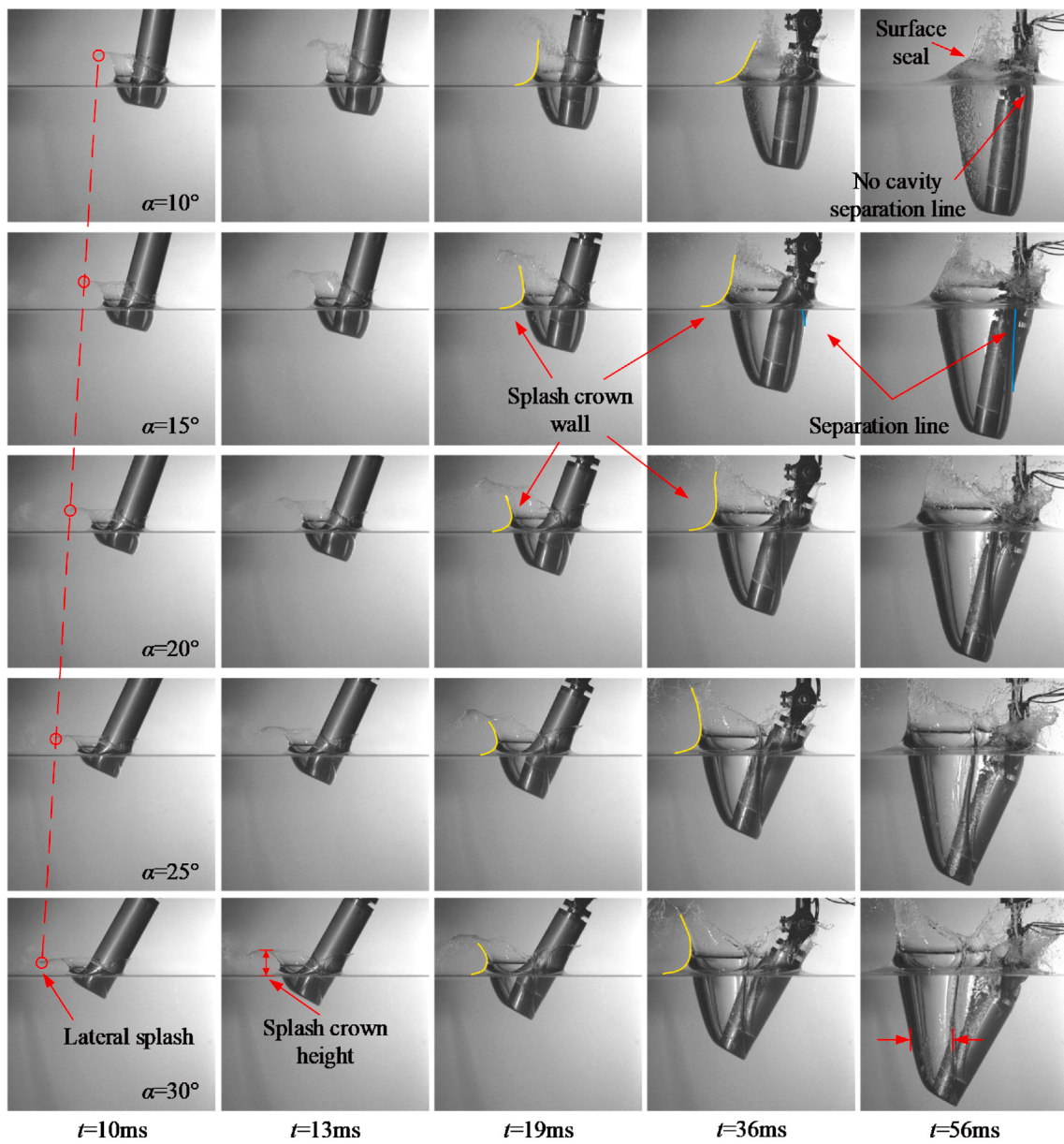
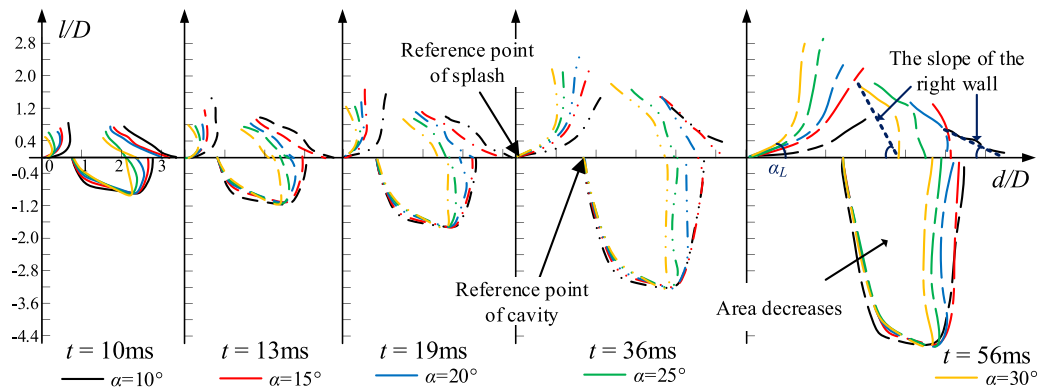


Fig. 9. Cavity evolution under different conditions.

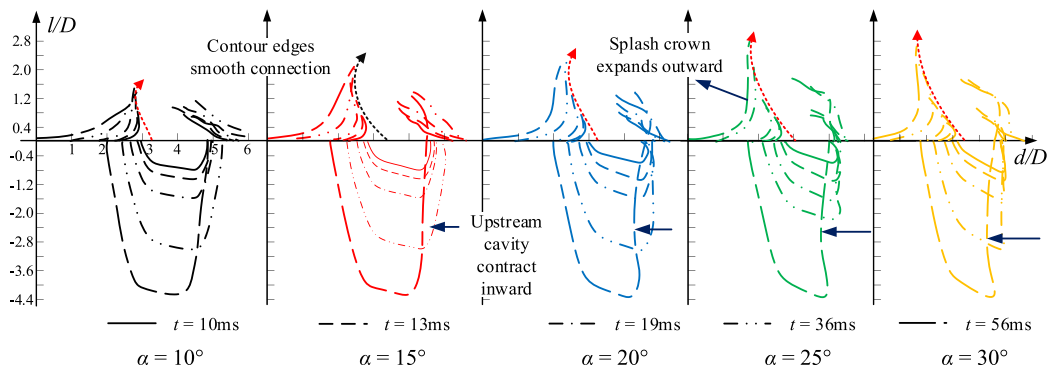
behavior of deformable spheres clearly differs from those of rigid spheres. Sun et al. (2019a; 2019b) carried out a series of experiments on sphere entry into a viscous liquid floating on water and studied cavity dynamics and splash crown behaviors under the influence of a viscous liquid. Li et al. (2020) studied the water entry of a spinning sphere by combining experiments and numerical calculations. They also provided a detailed analysis of the effects of spin rate on the flow evolution of a fluid and its dynamic characteristics. In practical engineering, the cylinder has a broad range of applications, so the focus of investigators gradually turned to the more practical area of studying the water entry of cylinders. Truscott et al. (2014) conducted a series of experiments on high-speed water entry, and their results showed that trajectory stability was severely affected by the angle of water entry. Wei et al. (2015) carried out a series of experiments on the water entry of circular cylinders in the low Froude numbers, and the cavity and hydrodynamic characteristics were analyzed in detail. Chen et al. (2019) focused on the stability of the trajectory of high-speed water-entry projectiles and showed that projectiles with a flat nose type exhibited perfect trajectory stability and maximum peak pressure. Guo et al. (2020) conducted an

experiment on the high-speed water entry of a projectile with a container constraint and produced analyses of the evolution of the cavity and changes in drag coefficient under the container constraint. Xia et al. (2019; 2020) studied the impact of cavities and motion behaviors in water entry using the motion of a cylinder with multiple degrees of freedom with different initial velocities and angles of inclination.

As a deeper understanding of the water entry problem developed, impact load became the research focus. The relationship between pressure and the cavity can be obtained by combining measurement results and test images. Abelson (1970) measured the pressure inside the cavity during the water entry of vertical and inclined projectiles and showed that the initial angle and nose shape of the projectile significantly affect internal cavity pressure. Van Nuffel et al. (2013; 2014) investigated the parameters that affect pressure recordings during water impact. The sampling rate, sensor position, temperature, surface conditions, and other parameters all affect pressures measurements. It was also found that Wagner's theory can estimate the impact pressure on a horizontal rigid cylinder accurately when the deadrise angle is larger than 4.25°. Alaoui et al. (2012; 2015) performed a series of experimental

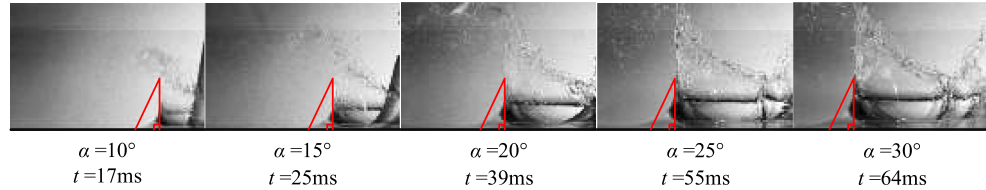


(a)

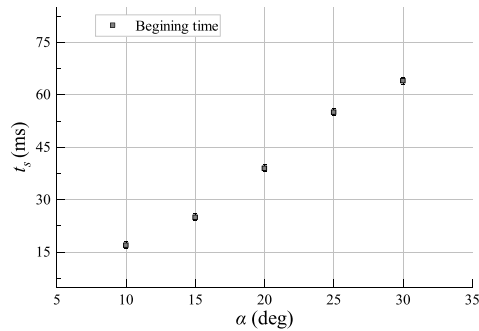


(b)

Fig. 10. Comparison of cavity and splash profiles: (a) with time as the abscissa and (b) with angle of attack as the abscissa.

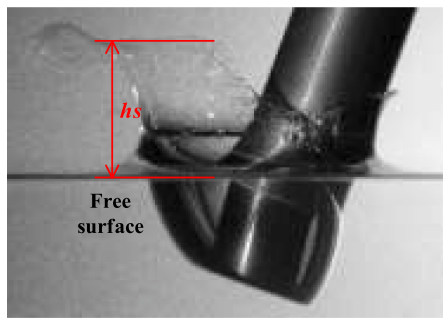


(a)

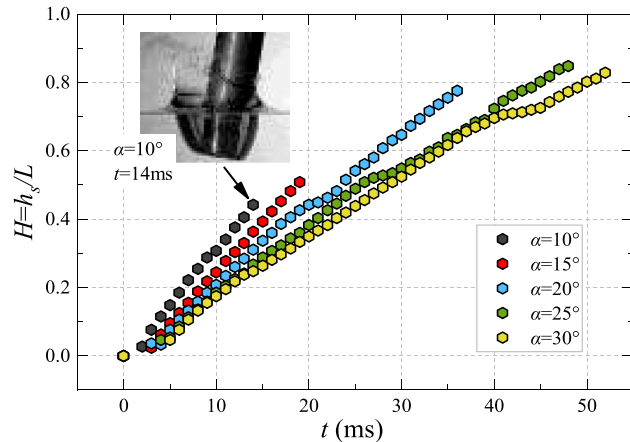


(b)

Fig. 11. Comparison of the moment when the crown begins to close t_s : (a) diagram of each working condition and (b) scatter plot and linear fitting curve.



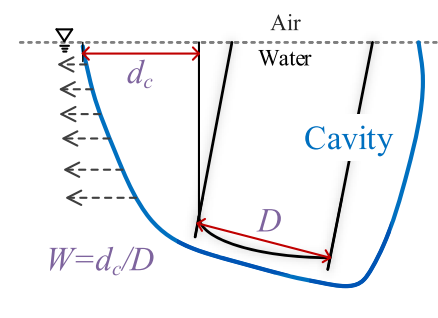
(a)



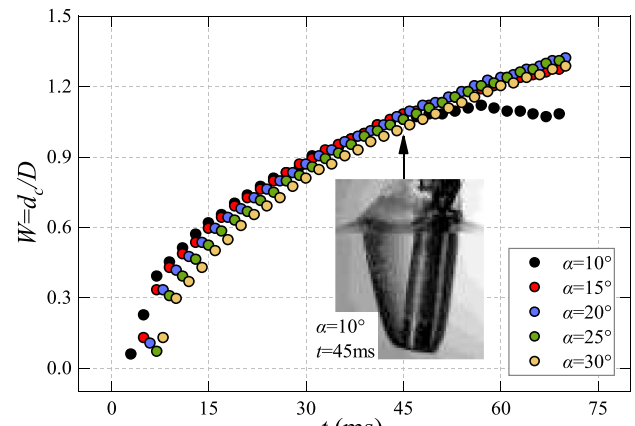
(b)

Fig. 12. Schematic diagram of the dimensionless height of splash crown H : (a) schematic diagram of h_s selection and (b) comparison of H values under different conditions.

investigations of the water entry of a pyramid, measured the resistance coefficient of vertical water entry, and obtained the relationship between impact pressure and velocity. Tenser et al. (2015) conducted an experiment investigation of impact loads and elastic deformations in wedge-shaped structures. Their results found values for impact pressures, accelerations, forces, and structural strains. Barjasteh et al. (2016) produced a study of the asymmetric water entry of wedges with different initial deadrise angles, inclination angles, and impact speeds. They showed that the inclination angle has a dramatic effect on the impact pressure that is experienced by the wedges. Nguyen et al. (2016; 2020) developed numerical model for multiphase flow with application to the water entry problem. Novel, the computational productivity was improved and the capability of the model in the accurate simulation of free surface and water-impact flows were demonstrated. Yang et al. (2017) studied the water entry of a vehicle in uncontrolled conditions, and they used an internal measurement system to analyze the characteristics of the vehicle's motion. Yan et al. (2018) conducted experiments on the water entry of Autonomous Underwater Vehicles using a range of velocities and angles and determining the results with high-speed photography and sensing technologies. Shi et al. (2019) used numerical and experimental methods to analyze cavity shapes and the load characteristics of the high-speed water entry of AUVs with different nose shapes and initial conditions. Malekmohammadi et al. (2019) studied and analyzed impact load characteristics of the water entry of two wedge shapes. They found that the shape of the model affected the sequence and frequency domain of the impact load. Zeraatgar et al. (2019) investigated the effects of sampling rate on impact pressure in



(a)



(b)

Fig. 13. Schematic diagram of the dimensionless width of the cavity: (a) schematic diagram for d_c selection and (b) comparison of W in different conditions.

experiments on the water entry of wedges. In some cases, smaller sampling rates could satisfy measurement requirements. Hasheminasab et al. (2019) presented a study of the water entry of twin wedges and measured the load characteristics. Based on the advantages of fluid-structure coupling method (Zhang et al., 2019), Sun et al. (2020) used the fluid-structure interaction method to analyze the structural response and load characteristics of high-speed water entry of a cylinder, and explained the structural damage caused by the impact load. Using pressure sensors, Treichler and Kiger (2020) studied the internal pressure characteristics of the supercavitation of projectiles in water the entry cavity. They showed that the size of the water tank significantly affected the dynamic characteristics of the cavity.

Although extensive research has been carried out on the cavity evolution and impact load of water entry, angle of attack as a variable parameter for the water entry of a cylinder is an important topic of in-depth study. Meanwhile, the inherent relationship between the load of the water entry structure and the flow field is of great significance for the study of the design of ships and marine structures. Here, we experimentally investigate the water entry of a constrained-posture cylinder with different angles of attack. Extracting test images and pressure curves from sensors distributed on the surface of the cylinder, we investigate the relationship between cavity and surface load. The relationship among angle of attack, cavity and load is explored by changing the angle of attack. Section 2 presents the experimental setup and the experimental conditions. Section 3 gives the experimental results and

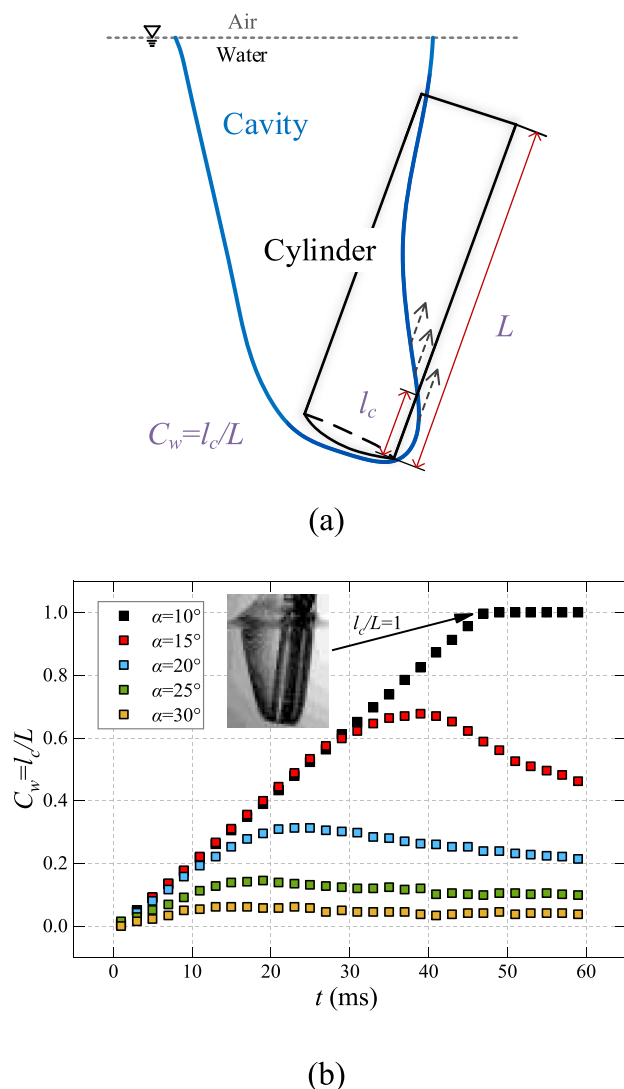


Fig. 14. Schematic diagram of cavity influence coefficient C_w : (a) schematic diagram of l_c selection and (b) comparison of C_w under different conditions.

analyzes the characteristics of the cavity, splash, and pressure under different angles of attack. The conclusions are presented in Section 4.

2. Experimental setup

Fig. 1 presents the schematic for our experimental system and the attitudes of the cylinder during the test. The upstream side of the cylinder is the first and fourth quadrant in the coordinate system, and the downstream side is the second and third quadrant. The entire system is divisible into four parts: release gear (electromagnet, sliding rail, and release switch), lighting device, high-speed camera, and measurement system. The water tank is $1400 \times 740 \times 800$ mm (length \times width \times height), and the water is 600 mm deep. Before each test, the electromagnet is electrified to fix the model connection device in place. When the release switch is turned off, the falls and begins water entry. Here, the high-speed camera begins to collect the images, and the measurement system records the pressure and acceleration of the entire process. A Phantom V12.1 high-speed camera is used, with a frame rate of 3000 fps and an image resolution of 1280×800 pixel.

The measurement system consists of three pressure sensors installed inside the cylinder, one external acceleration sensor, and an instrument for data acquisition. Fig. 2 shows the internal layout of the cylinder, which is divided into three parts to facilitate sensor installation. P1 is

placed at the center of the head of the cylinder, and the distances from P2 and P3 to the bottom of the cylinder are $0.38 D$ and $1.3 D$, respectively.

In order to verify the reliability of the test equipment, Fig. 3(a) shows the velocity curve during the water entry process for repeated test conditions. It can be seen that the velocity has a good consistency, and the maximum relative error is less than 2.5%. Moreover, Fig. 3(b) and (c) show the surface pressure curves of P2 and the images obtained based on three repetitive experiments for the 15° angle of attack respectively. These results indicate that the experiment has good repeatability.

The experimental conditions are summarized in Table 1. The initial velocity of water entry is extracted from the curves shown in Fig. 3. The attack angle of the cylinder is set using the angle adjuster and calibrated by the digital angle ruler to ensure that the angle of attack is consistent during the repeatability test. Each condition of the angle of attack is repeated at least three times to ensure measurement accuracy.

3. Results and discussion

3.1. Cavity evolution and load characteristics of the cylinder under a fixed angle of attack

To address cavity evolution and the surface load characteristics of cylinder water entry in relation to angle of attack, we provide detailed analyses of the conditions with an attack angle of $\alpha = 20^\circ$ and a velocity of $v_0 = 2.99$ m/s. Fig. 4 presents a sequence of images that depict the cavity evolution with the given condition. The first moment of contact between the cylinder and the free surface is defined as time zero ($t = 0$ ms). As the cylinder continues to fall, the water entry passes into the stage of flow formation at $t = 3$ ms. As a result of the entry transfer caused by the impact of the cylinder on free surface, the surrounding fluid acquires kinetic energy and begins to flow. At the same time, the cylinder bottom squeezes the discharged water, resulting in a lateral splash. The phase of flow formation is of very short duration and varies for different angles of attack. The open cavity stage occurs at $t = 10$ ms. As the water is pushed around, the air follows the entrainment of the cylinder, forming an obvious cavity and splash. At the same time, it is seen that the cavity in the downstream part is wholly connected with the atmosphere, while the cavity in the upstream part intersects with the cylinder and forms a semi-closed cavity due to asymmetry. An apparent splash crown and lateral jet are also observed due to extrusion. As time passes, the cavity downstream continues to expand, and the upstream cavity adheres to the surface of the cylinder, with a clear cavity-separation line gradually appearing. Because the air is constantly and quickly sucked into the cavity, the pressure inside the cavity is lower than the atmosphere, so the splash crown gradually shrinks inward. In the middle of the water entry, the top of the splash crown begins to collapse ($t = 35\text{--}45$ ms). Due to the reduced pressure difference between the interior of the cavity and the pressure of the atmosphere and the water, the wall of the stretched cavity upstream contracts inward and finally causes a deep pinch-off of the cavity. In the same way, the surface seal gradually occurs after the collapse of the splash crown.

Observation of the splash crown shows that the outer edge of the crown contracts toward the center before the surface seal. Fig. 5 presents this phenomenon and provides further analysis of the entire process. F and f represent the outward and inward force of the splash crown, respectively. h_c is the distance from the contour of the splash crown to the free surface, and l_s is the relative distance from the contour to the right vertex. It is well known that an inward force always occurs before the surface seal, due to the difference in internal and external pressure. However, the outward force caused by the energy exchange due to the impact of the water is far greater than the inward force. The opposite is true at the top of the splash crown. There, the inward force is slightly greater than the outward force, and this results in a trend in the movement of this position opposite to that of the whole crown. As time

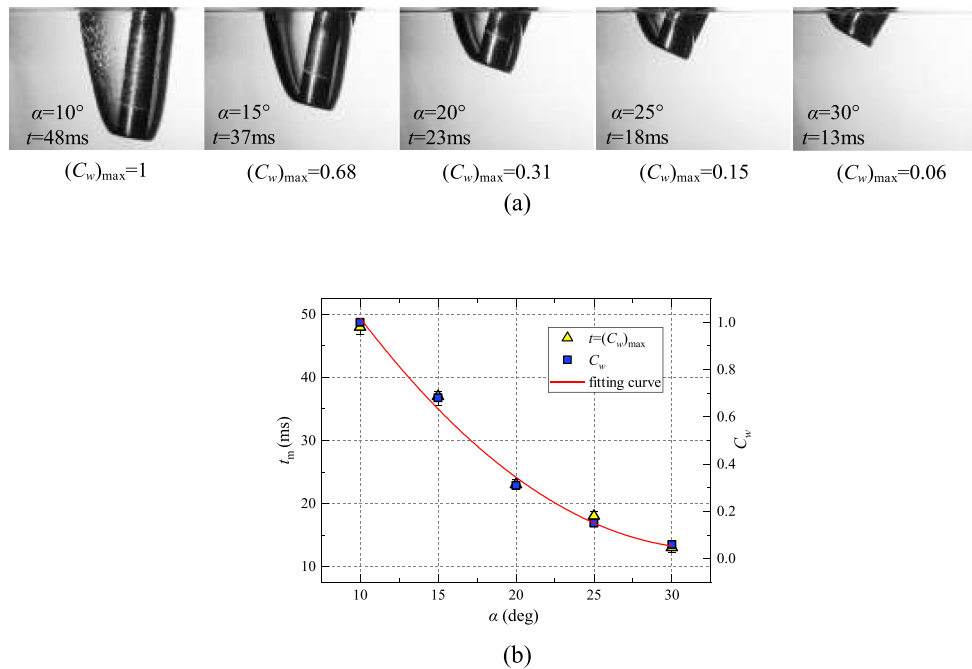


Fig. 15. Relationship among the moments when C_w reaches the maximum value of t_m , the maximum value of C_w , and time.

passes, the energy that is transferred due to the impact is gradually reduced, and the gap between the two forces narrows, such that the trend of outward expansion turns to an inward contraction. It is also seen that the top of the crown moves upward as it contracts. Fig. 5(b) connects the contour of the top of the splash crown (Marked by the red line in Fig. 5(a)) into a curved surface, which more intuitively reflects the law of the splash crown. It can be clearly seen that the evolution trend of the inward shrinkage and upward development of the splashes in time and space. Our analyses show that the imbalance between the outward and inward forces leads to a particular phenomenon at the top of the splash crown that is closely related to changes in force difference.

To explore the characteristics of the surface load of a constrained-posture cylinder with a certain angle of attack, we collect pressure signals at three points within this condition. First, Fig. 6 shows the curve of pressure versus time at P1. The overall change trend of the curve is the same as that of the typical water entry conditions, and all exhibit a rapid reduction to a lower stable value after the peak value is reached. When $t = 0$ ms, the cylinder contacts the free surface for the first time, and due to the angle of attack, P1 is still a certain distance from the surface of the water, so the pressure at P1 is approximately equal to the current ambient pressure. The pressure reaches a peak value at $t = 2$ ms, and P1 impacts the free surface. When $t = 15$ ms, the cylinder passes through water impact, the interaction between P1 and the water changes from impact to continuous contact under the action of water resistance and water pressure, and the pressure at P1 is continuously and stably higher than atmospheric pressure. Thus, we can judge the mechanism of the peak water entry pressure in relation to the angle of attack, and the time of peak pressure occurs at the same velocity for both the vertical and inclined conditions.

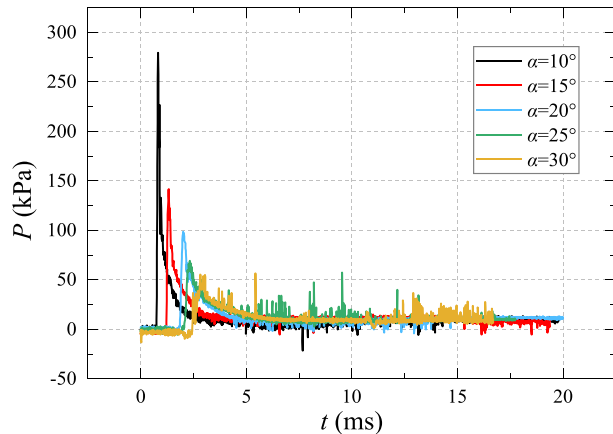
The pressure curve for P2 and images of four characteristic moments are given in Fig. 7. The entire pressure curve increases rapidly, attains peak pressure at a relatively slow speed, and finally decreases to approximately ambient pressure. There is noticeable pressure fluctuation during the second increase. No obvious pressure variation appears during $t = 0\text{--}4$ ms, indicating that the impact has no influence on P2. The pressure rises rapidly due to contact with the free surface ($t = 4$ ms). The cylinder wall forms a 70° angle with the surface of the water, so the force of the impact has a small component on the wall, and the pressure is mainly generated by contact with the water. At the same time, the

upstream cavity has no noticeable effect on P2. As the water pressure increases, the pressure at P2 also gradually increases. Meanwhile, we can see that the pressure sharply decreases during 6–6.8 ms. The surface pressure is affected by the cavity splash around the cylinder, and presents fluctuation characteristics. The upstream cavity separation line just passes the sensor surface during this period, and the pressure reaches its peak value after that. As the cavity covers the head of the cylinder, including P2, the pressure drops to the range of the environmental pressure. The curves shown in Figs. 6 and 7 show different trends, indicating that the impact load and surface load for cylinder water entry at a given angle of attack are significantly different.

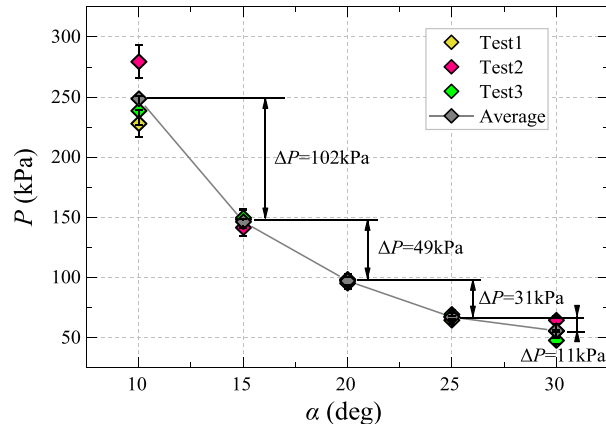
Finally, pressure of P3 is shown in Fig. 8. Because P3 is far from the bottom of the cylinder, the pressure curve shows no visible change. When $t = 11.6$ ms, a positive pressure trend is seen. The images show that P3 comes into contact with the water attached to the wall due to the splash, so pressure increases during this period. Similarly, when P3 is in contact with the surface of the water, the pressure increases accordingly. Interestingly, it can be seen that the pressure evolution of P3 presents negative values after 12 ms. During the water entry process of cylinder, the air around the cylinder is driven to flow and form cavitation splash. Cavity seal around the cylinder prevents entrained air flowing into the cavity, thus causing the measured pressure to be lower than the ambient atmospheric pressure.

3.2. Influence of angle of attack on cavity evolution and splash

In this section, the evolution of the cavity and the characteristics of the splash in the process of cylinder water entry with angles of attack 10° , 15° , 20° , 25° , and 30° are analyzed. First, we analyze the entire process of water entry. Fig. 9 shows a sequence of images of cavity evolution in different conditions. Because the cylinder's rotation is constrained, the rotating moment caused by water resistance is not taken into consideration. The impact of the angle of attack is mainly reflected in the lateral splash, the height of the splash crown, and the surface seal, as well as in the area of the cavity, cavity separation line, and other phenomena. The impact of the lateral splash can be seen in a comparison to the image for $t = 10$ ms. Under conditions of a higher angle of attack, the horizontal component of the impact force is larger, and more energy is transferred to the water. Hence, the distance of



(a)

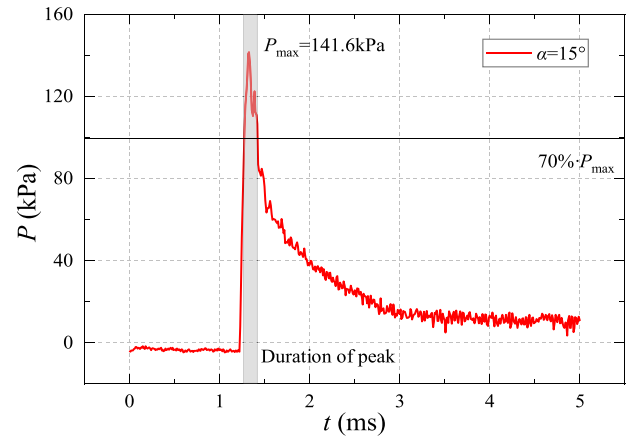


(b)

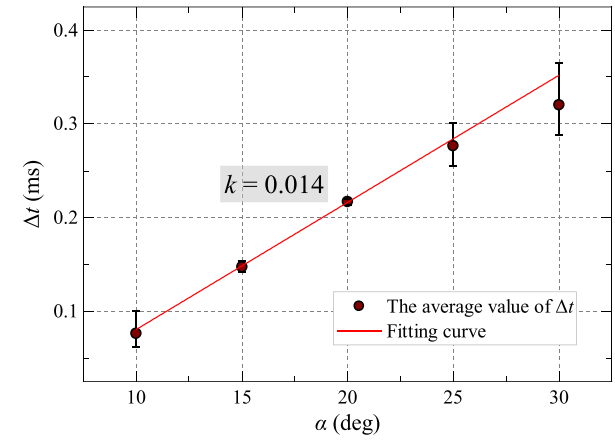
Fig. 16. Comparison of P1 pressure under different conditions: (a) complete pressure curve for water entry and (b) peak pressure and average peak pressure for repeated tests.

lateral splash increases with increases in angle of attack. Given the same entry velocity, increases in the horizontal component represent decreases in the vertical component, such that when $t = 13$ ms, the 10° angle of attack has the highest splash crown height, which decreases with increases in attack angle. Furthermore, because horizontal energy affects the contraction seal of the splash crown, the surface seal occurs much later for higher attack angles. Analyses of the cavity show that the appearance time of upstream cavity separation line decreases with increases in the attack angle, also indicating that the greater the attack angle, the smaller the area of influence of upstream cavity on the cylinder surface. An upstream cavity in the 10° attack angle completely surrounds the cylinder ($t = 56$ ms), so it can be concluded that the time of cavity pinch-off is the latest, and the earlier the cavity separation, the shorter the time to cavity pinch-off.

In order to address the evolution features of cavity splash, we extract the cavity profiles based on image enhancement and edge detection operators method. Fig. 10 gives comparative analyses in relation to different moments and different angles of attack, represented by different line types and colors, respectively. l and d respectively



(a)



(b)

Fig. 17. Relationship between duration of high load and attack angles: (a) schematic of Δt selection and (b) scatter diagram Δt of with α .

represent the vertical distance between the contour and the free surface and the horizontal distance between the contour and the reference point of splash. Fig. 10(a) takes time as the horizontal axis. For convenience, different reference points are selected for the splash crown and the cavity. The contrast of the contour of the splash crown indicates that with the increase of the angle of attack, the angle α_L between the left wall of the crown and the free surface increases, the right wall moves toward the middle, and the absolute value of the slope of the right wall gradually increases. From a comparison of the contour of the cavity, the change rule for the right wall of the cavity is the same as that for the splash crown. As the attack angle increases, the area of the cavity decreases at the same moment. Fig. 10(b) takes the attack angle as the horizontal axis. Unlike vertical and inclined water entry, the wall of the upstream cavity shows a trend toward inward contraction, and the larger the angle of attack, the more obvious this trend is. With increases in time, the left wall of the splash crown expands outward, and the top contour of the crown is related to the angle between the initial crown wall and the free surface. The influence of the angle of attack on the surface seal can be further analyzed. Analyses of the cavity and splash evolution and comparison of the extracted contours lead to a certain understanding of the impact of different angles of attack on the entire process of water entry. Next, we conduct an in-depth study of specific parameters of the cavity and splash.

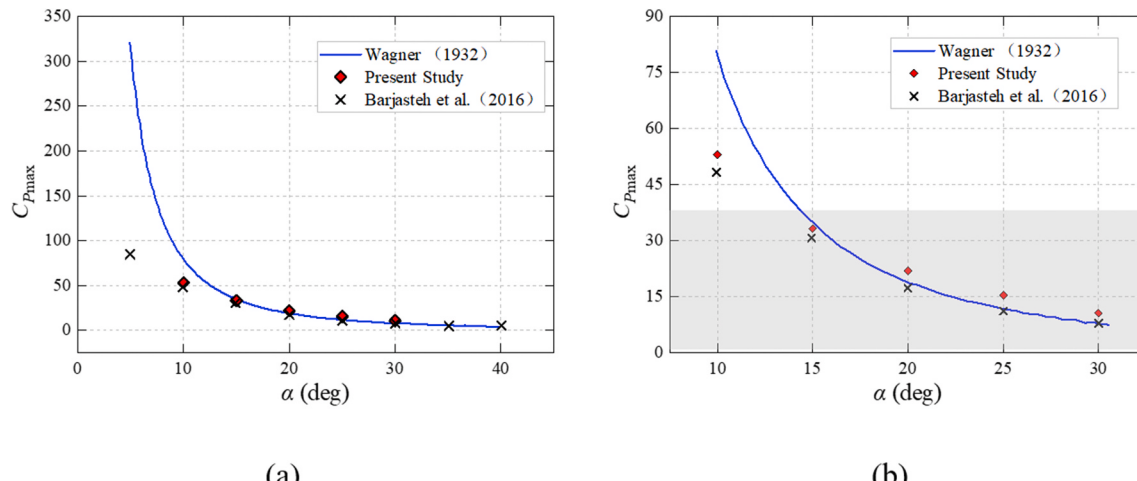


Fig. 18. Comparison of maximum pressure coefficients with a theoretical model and previous results: (a) complete view and (b) partial magnified view.

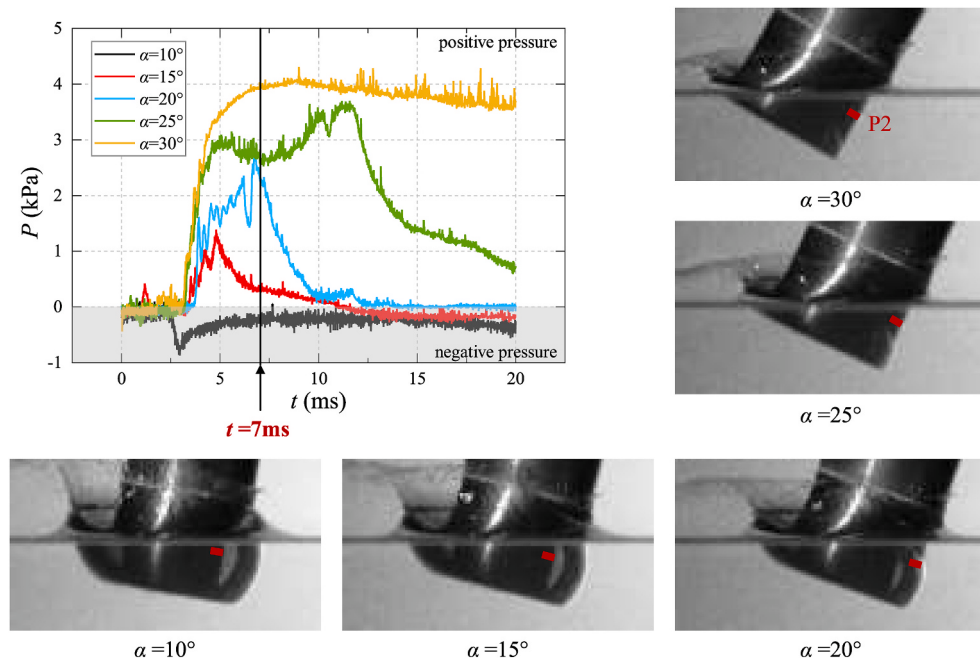


Fig. 19. Schematic diagram of experiment images at specific time ($t = 7 \text{ ms}$).

Fig. 11 presents images of the moment when the crown begins to close (t_s) under different conditions and a scatter diagram for t_s . Here, t_s increases with increases in the angle of attack in an approximately linear fashion.

We select several characteristic quantities for comparative analyses. First, the ratio of the height of the splash crown h_s to the length of cylinder L is selected to describe the dimensionless height H of the crown. The schematic diagram for the method of h_s selection and the scatter diagram for the changes in H over time in different conditions are shown in **Fig. 12**. H increases approximately linearly with time. Combined with the above analyses of t_s , it is clear that the time of collapse at the top of splash crown increases with the increase in attack angle. At a 10° angle of attack, there is no visible top for the splash crown at about 13 ms, but in the 30° condition, the top persists until about 52 ms. At the same time, the contact area between the small attack angle condition and the free surface is larger than for the large attack angle condition, so the energy exchange is greater for the small attack angle. That is, the faster H increases, the more the slope decreases with increases in the angle of

attack. Analyzing the parameters of the splash crown shows that in the range of angle of attack selected in the experiment, the start time of the inward contraction of the crown increases approximately linearly with the angle of attack. Accordingly, the time of crown collapse is the earliest for 10° , and the growth rate of the splash crown increases with increases in the attack angle.

The ratio of the distance from the left end of the cavity to the left end of the cylinder d_c to the diameter of the cylinder D is selected as to represent the dimensionless width of the cavity W . **Fig. 13** gives a schematic diagram of W and the scatter diagram in different conditions. The overall trend shows that cavity width W increases over time, but the growth rate decreases only gradually. The initial value for W occurs later than the small angle of attack due to the late occurrence of the open cavity stage in the high angle of the attack condition, and the high attack angle condition is accompanied by greater horizontal component force. In this case, the growth rate of W at the initial water entry is faster. Because the crown closing time is the earliest at 10° , completed in 50 ms, and the inward contraction force significantly inhibits the development

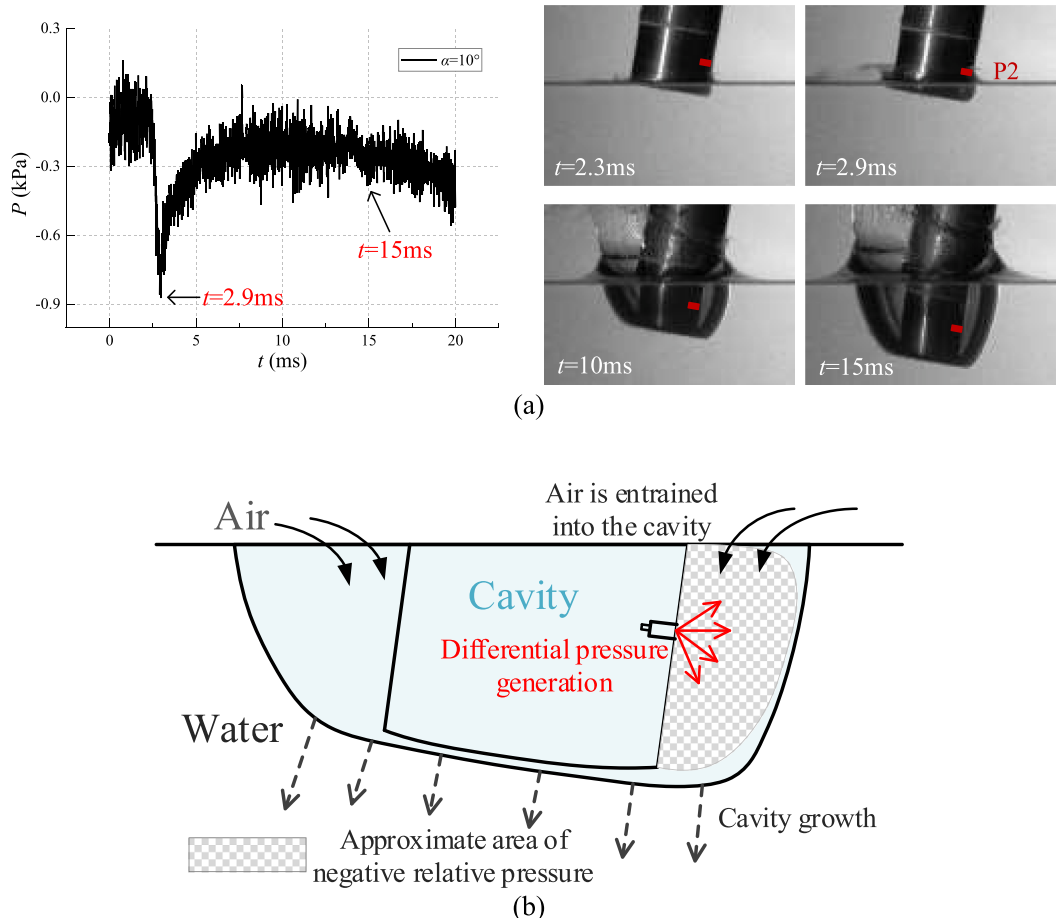


Fig. 20. Schematic diagram of pressure at P2 for $\alpha = 10^\circ$: (a) pressure curve and experimental images of characteristic moments and (b) schematic diagram to explain negative relative surface pressure.

of the cavity, the width curve for the cavity in this condition exhibits a different trend than that of other conditions after 45 ms.

The influence area of the cavity on the cylinder wall differs in relation to the differently asymmetric characteristics of the cavity at different angles of attack. To study the influence area of the cavity, we assign the cavity influence coefficient C_w to the ratio of the length of upstream cavity wrapped cylinder l_c to the cylinder length L . Fig. 14 shows the schematic diagram and scatter diagram for C_w . A trend of first increasing to a stable range and then decreasing is seen. The cavity on the upstream side at 10° completely envelops the cylinder, so C_w reaches its maximum value of 1 at 48 ms. It is also seen from a comparison of the curves that increases in the attack angle significantly reduce the cavity's area of influence on the cylinder, and the time to reach its maximum value is delayed. In addition, the speed of decrease for C_w gradually increases.

Next, we extract the moment when the upstream cavity influence coefficient reaches its maximum value t_m under different angles of attack conditions. Fig. 15 shows images of the cavity at t_m and a scatter diagram of t_m and $(C_w)_{\max}$, respectively. Both obviously decrease with increased angle of attack. The curve in Fig. 15(b) shows the curve after second-order polynomial fitting, and it demonstrates that $(C_w)_{\max}$ and t_m present similar trends.

3.3. Influence of angle of attack on the impact and surface load

This section investigates the influence of different angles of attack on the impact and surface pressures of the cylinder. First, we study the head of the cylinder that bears the largest load during water entry, and the P1 pressure curve for different conditions is extracted in Fig. 16. At the

same time, to obtain more accurate results and to verify the repeatability of the measurements, the maximum and average values for impact pressure in the three groups of tests at each angle of attack are also shown in Fig. 16. A comparison of the pressure curves for different conditions shows that the influence of angle of attack on P1 pressure is reflected in the peak value and the time that the peak value appears. Because of the large vertical distance between P1 and the free surface at a high angle of attack, the peak value for P1 appears later at the same speed of water entry. Fig. 16(b) indicates more intuitively that the peak value for impact load at P1 shows an obvious decrease for increases in attack angle. Compared to the difference between the average value of the peak pressure of adjacent attack angle, it can be seen that the difference shows a trend of approximate gradient change.

The research consensus is that both speed and angle of water entry affect the duration of high load, so we will take 70% of the peak pressure of the impact load in each condition as the standard value and define the duration of high load Δt as the time when the pressure value is above the standard value. Fig. 17(a) shows a schematic diagram of the extraction of the high load duration. The average value of Δt in Fig. 17(b) shows that the duration of the high load increases with increases in the attack angle. At the same time, linear fitting shows an approximately linear relationship between Δt and α . The above analyses of the impact load and the duration of high load at the center of the bottom of the cylinder at different attack angles show the peak value of the impact pressure decreases in a gradient fashion with increases in attack angle. By comparing the duration of high load during water entry, we find that the relationship between the duration of high load and angle of attack is approximately linear.

To evaluate the reliability of the results, it is necessary to compare

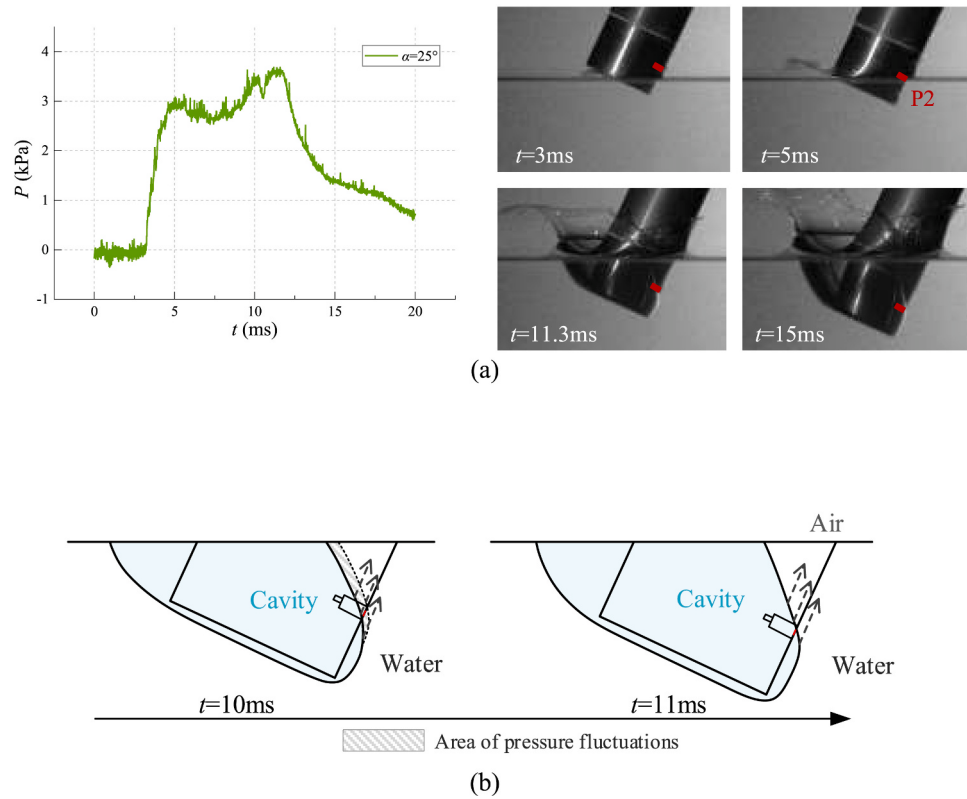


Fig. 21. Schematic diagram of the pressure at P2 at $\alpha = 25^\circ$: (a) pressure curve and images of characteristic moments and (b) schematic diagram of pressure fluctuation.

the test results with existing research. The function to be compared is the maximum pressure coefficient, estimated with the following expression:

$$C_{P_{\max}} = \frac{P_{\max}}{0.5\rho_w v_0^2} \quad (1.1)$$

where v_0 is the impact velocity obtained from the acceleration integral, and P_{\max} is the peak value of the pressure curve. Fig. 18 compares the maximum pressure coefficients with the Wagner (1932) Model and the experimental results produced by Barjasteh et al. (2016). A good agreement is found with Barjasteh et al. (2016), and the Wagner (1932) model for attack angles greater than 15° . This matches the law obtained by Barjasteh et al. (2016), largely due to the assumptions of Wagner's model. Due to the assumptions of the model, air drag and the buffer effect are not considered in the simple Wagner model. Thus, this theory overestimates the maximum pressure coefficient for small angles of attack.

To explore changes in surface load as a cylinder enters water with an angle of attack, we extract the measurement results for the P2 pressure sensor under different conditions and choose the images at the moment ($t = 7$ ms) when the pressure for each condition has obvious differences. The curves and images of the cavity at that moment are shown in Fig. 19. We find that pressure variations in P2 are different from those of P1, which indicates an obviously different tendency for different angles of attack, mainly reflected in differences in pressure value and time domain. At $t = 7$ ms, pressure at P2 is less than atmospheric pressure for a 10° attack angle, and the relative pressure is negative. This image shows that P2 is in the interior of the cavity, and the cavity is connected with the air. Due to the sudden expansion of the cavity, less air flows in, so the pressure in the cavity is less than the atmosphere, and the absolute value of the relative pressure at P2 is at its peak. Due to the continuous inflow of air, the pressure difference is reduced, and the absolute value of the pressure at P2 becomes less than its value at the beginning of cavity development. For the 15° condition, the pressure is slightly

greater than atmospheric pressure. Although the upstream cavity wraps around the cylinder head, there is no visible cavity on the right side. The pressure at the 20° angle of attack passes the peak value and begins to show a downward trend. It is clear that the upstream cavity-separation line is just at the upper end of P2. Although P2 shows positive pressure at a 25° angle of attack, a downward trend nevertheless appears. The cavity separation line nears the lower side of P2 at that moment. At the same moment, at 30° , the pressure is close to its peak value, and there is a trend toward continuous increase. P2 is entirely in contact with water and is not affected by the cavity. In Fig. 20, we see that changes in surface load are different from those in impact load. By selecting specific times and performing individual analyses of different conditions, we obtain a preliminary understanding of the reasons for changes in surface load. We select three surface load curves for detailed description.

To further explain the change law for pressure at P2 in relation to different angles of attack, three representative conditions are that indicate the relationship between cavity and load, and the results for negative values, positive values, and pressure fluctuations are analyzed. First, the pressure curve for P2 for 10° is given separately in Fig. 20, and experimental images of four typical moments are given on the right side in that figure. When $t = 2.3$ ms, no obvious cavity appears because the cylinder has just passed water impact. A certain distance remains between P2 and free surface, but because the impact with water causes violent flow field movement a small pressure fluctuation results. At $t = 2.9$ ms, a cavity is generated at the head of cylinder, and P2 is in the interior of the cavity. Because air is entrained into the cavity in water entry due to pressure differences, the internal pressure of the cavity is less than atmospheric pressure. Thus, the pressure at P2 is significantly less than atmospheric pressure. As upstream cavity expands, P2 has negative pressure, but because of the continuous entry of air, the pressure difference decreases, and the absolute value of the pressure is small. At a 10° angle of attack, the pressure change in P2 leads to a surface load of the cylinder that is less than atmospheric pressure at water entry

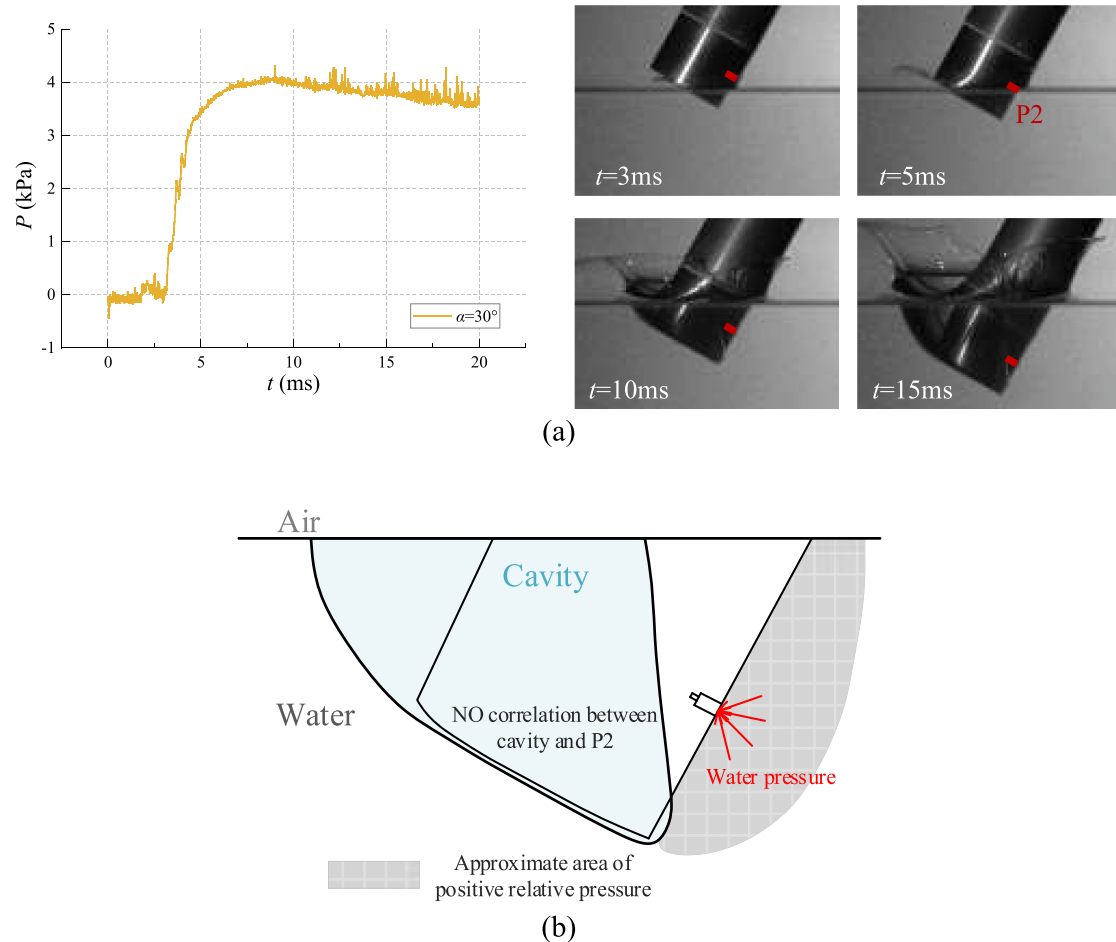


Fig. 22. Schematic diagram of the pressure at P2 at $\alpha = 30^\circ$ (a) pressure curve and images of characteristic moments and (b) schematic diagram to explain the positive relative surface pressure.

because of the generation and development of the cavity. The continuous inflow of air causes the interior of the cavity to reach negative pressure. Fig. 21(b) presents this phenomenon in a schematic diagram. It should be noted that the shadow area in the figure is an approximate area of negative pressure, which is only used to explain the pressure change near P2.

Fig. 21 presents the pressure curve of P2 for a 25° angle of attack and corresponding images of typical moments. No obvious law governs the pressure change. The reasons for the pressure change are analyzed in combination with the cavity images below. At $t = 3$ ms, the cavity appears on the upstream side, and P2 remains some distance from the free surface, meaning that the pressure here is near to atmospheric pressure. The first peak of the curve appears at $t = 5$ ms. The image indicates that P2 impacts the water surface, and the principle that generates load is similar to that of the center of the bottom surface. Because an instantaneous increase in the cavity volume leads to suction, the pressure shows a short-term decreasing trend. During $t = 10\text{--}11$ ms, the pressure has obvious fluctuations. Observation of the change in cavity indicates that the upstream cavity separation line sweeps the sensor surface of P2. Therefore, the fluctuation of the pressure curve is due to the sweeping of the separation line. Fig. 22(b) gives a schematic diagram to explain this. When $t = 15$ ms, the upstream cavity covers the surface of the cylinder, including P2. The pressure change inside the cavity is analyzed above. The theory still applies, and pressure shows a decreasing trend at this moment.

Fig. 22(a) shows the pressure curve for P2 and the cavity images at characteristic moments for the 30° angle of attack. For $t = 3$ ms, P2 does not contact the water surface, and there is no obvious cavity. The flow

field in contact with the P2 sensor is mainly air, so pressure remains approximately equal to ambient pressure. At $t = 5$ ms, the upstream cavity still does not affect the P2 sensor, but P2 is in contact with the free surface, so its pressure is about to reach the peak value. We know that the maximum value of the cavity influence coefficient is 0.06 at the upstream side of 30° angle of attack, which means that the cavity generated upstream does not pass through the sensor surface during water entry. Therefore, P2 is in direct contact with the water, so the relative pressure is positive, and there is no noticeable pressure fluctuation. Analyses of P2 pressure change for $\alpha = 30^\circ$ show why surface load presents a stable positive value during water entry at different angles of attack. Fig. 22(b) presents a schematic diagram to help explain this phenomenon. When P2 is in direct contact, water pressure acts on the surface of the sensor, resulting in positive relative pressure at the location. If there is no cavity effect, the pressure curve does not fluctuate significantly. Similarly, the shaded area in the figure is also a schematic area to show the pressure change near P2 in this condition.

4. Conclusions

We experimentally study the evolution of the cavity and splash and the load characteristics of water entry with initial conditions of different angles of attack. The main conclusions of the present study are as follows:

- (1) The characteristics of the flow field play an important role in the surface load of the cylinder. The cavities evolution over time shows obvious unsteady characteristics, and is characterized as

- cavity formation, development, separation, collapse, and necking, etc. Meanwhile, the internal and external pressure environment and mechanical properties dominate the evolution of the cavity. The pressure on the head of the cylinder shows a clear peak, but the pressure load on the shoulder of the cylinder is reduced and shows more complex pulsation characteristics.
- (2) Cavity evolution during the water entry process is closely related to the angle of attack of the cylinder. Larger angles of attack shorten the time of cavity pinch-off but extend the time of surface seal. The time that the splash crown begins to shrink inward shows an approximately linear relationship to the angle of attack. The growth rate of the splash crown decreases with increases in attack angle, and the change law of the cavity width has the opposite tendency. The influence coefficient of the upstream cavity decreases as the attack angle increases, and the peak value of the coefficient and the moment of reaching the peak value show the same change law.
- (3) The angle of attack of the cylinder has a significant effect on the load characteristics of water entry. The peak value of impact pressure shows a downward trend in the test conditions, and the moment of the peak value appear is delayed. Moreover, it is found that the relationship between the duration of high load and the angle of attack has a linear increase. For the surface load of the cylinder, entrained air at an initial stage of water entry process causes the relative pressure of the surface inside the cavity is momentarily negative. When the cavity separation line passes the model surface, the surface has undergone drastic changes in the flow field and a pressure fluctuation appears. The part in contact with the water shows significant positive pressure due to the pressure of water.

CRediT authorship contribution statement

Tiezhi Sun: Conceptualization, Methodology, Formal analysis, Data curation, Writing - original draft, Writing - review & editing, Project administration, Funding acquisition, Supervision. **Chongbin Shi:** Investigation, Formal analysis, Data curation, Formal analysis, Writing - original draft, Writing - review & editing. **Guiyong Zhang:** Conceptualization, Resources, Writing - original draft, Writing - review & editing, Project administration, Funding acquisition. **Zhi Zong:** Conceptualization, Methodology, Writing - review & editing, Project administration. **Heng Wang:** Experiment, Formal analysis, Writing - original draft, Writing - review & editing.

Declaration of competing interest

The authors declare that they have no known competing financial interests or personal relationships that could have appeared to influence the work reported in this paper.

Acknowledgments

This work was supported by the National Natural Science Foundation of China (51709042, 52071062, 51679037, 51639003), the China Postdoctoral Science Foundation (2019T120211, 2018M631791), the Natural Science Foundation of Liaoning Province of China (2020MS106), the 2018QNRC001, the Liao Ning Revitalization Talents Program (XLYC1908027), and the Fundamental Research Funds for the Central Universities (DUT20TD108, DUT20LAB308).

References

- Abelson, H.I., 1970. Pressure measurements in the water-entry cavity. *J. Fluid Mech.* 44 (1), 129–144.
- Alaoui, A.E.M., Neme, A., Tassin, A., Jacques, N., 2012. Experimental study of coefficients during vertical water entry of axisymmetric rigid shapes at constant speeds. *Appl. Ocean Res.* 37, 183–197.
- Alaoui, A.E.M., Neme, A., Scolan, Y.M., 2015. Experimental investigation of hydrodynamic loads and pressure distribution during a pyramid water entry. *J. Fluid Struct.* 54, 925–935.
- Aristoff, J.M., Truscott, T.T., Techet, A.H., Bush, J.W., 2008. The water-entry cavity formed by low Bond number impacts. *Phys. Fluids* 20 (9), 091111.
- Aristoff, J.M., Bush, J.W., 2009. Water entry of small hydrophobic spheres. *J. Fluid Mech.* 619, 45–78.
- Barjasteh, M., Zeraatgar, H., Javaherian, M.J., 2016. An experimental study on water entry of asymmetric wedges. *Appl. Ocean Res.* 58, 292–304.
- Bell, G.E., 1924. LXVI. On the impact of a solid sphere with a fluid surface and the influence of surface tension, surface layers, and viscosity on the phenomenon. *London Edinburgh Philos. Mag. J. Sci. London, Edinburgh Dublin Philos. Mag. J. Sci.* 48 (287), 753–764.
- Chen, T., Huang, W., Zhang, W., Qi, Y., Guo, Z., 2019. Experimental investigation on trajectory stability of high-speed water entry projectiles. *Ocean Eng.* 175, 16–24.
- Ding, H., Chen, B.Q., Liu, H.R., Zhang, C.Y., Gao, P., Lu, X.Y., 2015. On the contact-line pinning in cavity formation during solid-liquid impact. *J. Fluid Mech.* 783, 504–525.
- Duez, C., Ybert, C., Clanet, C., Bocquet, L., 2007. Making a splash with water repellency. *Nat. Phys.* 3 (3), 180–183.
- Gilbarg, D., Anderson, R.A., 1948. Influence of atmospheric pressure on the phenomena accompanying the entry of spheres into water. *J. Appl. Phys.* 19 (2), 127–139.
- Greenhow, M., 1987. Wedge entry into initially calm water. *Appl. Ocean Res.* 9 (4), 214–223.
- Guo, Z., Chen, T., cheng Mu, Z., Zhang, W., 2020. An investigation into container constraint effects on the cavity characteristics due to high-speed projectile water entry. *Ocean Eng.* 210, 107449.
- Hasheminasab, H., Zeraatgar, H., Moradi, H., Sakaki, A., 2020. Experimental study on water entry of twin wedges. *Proc. IME M J. Eng. Marit. Environ.* 234 (2), 388–398.
- Hurd, R.C., Belden, J., Jandron, M.A., Fanning, D.T., Bower, A.F., Truscott, T.T., 2017. Water entry of deformable spheres. *J. Fluid Mech.* 824, 912–930.
- Lee, M., Longoria, R.G., Wilson, D.E., 1997. Cavity dynamics in high-speed water entry. *Phys. Fluids* 9 (3), 540–550.
- Li, D., Zhao, X., Kong, D., Shentu, J., Wang, G., Huang, B., 2020. Numerical investigation of the water entry of a hydrophobic sphere with spin. *Int. J. Multiphas. Flow* 126, 103234.
- May, A., Woodhull, J.C., 1948. Drag coefficients of steel spheres entering water vertically. *J. Appl. Phys.* 19 (12), 1109–1121.
- May, A., 1951. Effect of surface condition of a sphere on its water-entry cavity. *J. Appl. Phys.* 22 (10), 1219–1222.
- May, A., 1952. Vertical entry of missiles into water. *J. Appl. Phys.* 23 (12), 1362–1372.
- Malekmohammadi, J., Zeraatgar, H., Hasheminasab, H., 2019. Performance comparison of ordinary-chine wedges with flat-chine wedges in water entry problem. *Ships Offshore Struct.* 1–10.
- Nguyen, V.T., Vu, D.T., Park, W.G., Jung, C.M., 2016. Navier–Stokes solver for water entry bodies with moving Chimera grid method in 6DOF motions. *Comput. Fluids* 140, 19–38.
- Nguyen, V.T., Thanh-Hoang, P., Park, W.G., 2020. Modeling and numerical simulation of ricochet and penetration of water entry bodies using an efficient free surface model. *Int. J. Mech. Sci.* 182, 105726.
- Richardson, E.G., 1948. The impact of a solid on a liquid surface. *Proc. Phys. Soc.* 61 (4), 352.
- Shi, Y., Pan, G., Yan, G.X., Yim, S.C., Jiang, J., 2019. Numerical study on the cavity characteristics and impact loads of AUV water entry. *Appl. Ocean Res.* 89, 44–58.
- Sun, T., Wang, H., Zong, Z., Zhang, G., Wang, A., Xu, C., 2019a. Splash formation and cavity dynamics of sphere entry through a viscous liquid resting on the water. *AIP Adv.* 9 (7), 075211.
- Sun, T., Wang, H., Zou, L., Zong, Z., Li, H., 2019b. Experimental study on the cavity dynamics of oblique impact of sphere on a viscous liquid floating on water. *Ocean Eng.* 194, 106597.
- Sun, T., Zhou, L., Yin, Z., Zong, Z., 2020. Cavitation bubble dynamics and structural loads of high-speed water entry of a cylinder using fluid-structure interaction method. *Appl. Ocean Res.* 101, 102285.
- Truscott, T.T., Techet, A.H., 2009. Water entry of spinning spheres. *J. Fluid Mech.* 625, 135–165.
- Truscott, T.T., Epps, B.P., Belden, J., 2014. Water entry of projectiles. *Annu. Rev. Fluid Mech.* 46, 355–378.
- Treichler, D.M., Kiger, K.T., 2020. Shallow water entry of supercavitating darts. *Exp. Fluid* 61 (2), 31.
- Tenzer, M., Moctar, O.E., Schellin, T.E., 2015. Experimental investigation of impact loads during water entry. *Ship Technol. Res.* 62 (1), 47–59.
- Verhagen, J.H.G., 1967. The impact of a flat plate on a water surface. *J. Ship Res.* 11, 211–223, 04.
- Von Karman, T., 1929. The Impact on Seaplane Floats during Landing.
- Van Nuffel, D., Vepa, K.S., De Baere, I., Degrieck, J., De Rouck, J., Van Paepengem, W., 2013. Study on the parameters influencing the accuracy and reproducibility of dynamic pressure measurements at the surface of a rigid body during water impact. *Exp. Mech.* 53 (2), 131–144.
- Van Nuffel, D., Vepa, K.S., De Baere, I., Lava, P., Kersemans, M., Degrieck, J., Van Paepengem, W., 2014. A comparison between the experimental and theoretical impact pressures acting on a horizontal quasi-rigid cylinder during vertical water entry. *Ocean Eng.* 77, 42–54.
- Wagner, H., 1932. Phenomena associated with impacts and sliding on liquid surfaces. *Z. Angew. Math. Mech.* 12 (4), 193–215.
- Wei, Z., Hu, C., 2015. Experimental study on water entry of circular cylinders with inclined angles. *J. Mar. Sci. Technol.* 20 (4), 722–738.

- Worthington, A.M., Cole, R.S., 1897. V. Impact with a liquid surface, studied by the aid of instantaneous photography. *Philos. trans. R. Soc. Lond. Series A, Containing Papers of a Mathematical or Physical Character* 189, 137–148.
- Xia, W., Wang, C., Wei, Y., Li, J., 2019. Experimental study on water entry of inclined circular cylinders with horizontal velocities. *Int. J. Multiphas. Flow* 118, 37–49.
- Xia, W., Wang, C., Wei, Y., Li, J., Li, Y., Yang, L., 2020. Position detection method and hydrodynamic characteristics of the water entry of a cylinder with multidegree motion. *Exp. Fluid* 61 (2), 57.
- Xu, G.D., Duan, W.Y., Wu, G.X., 2008. Numerical simulation of oblique water entry of an asymmetrical wedge. *Ocean Eng.* 35 (16), 1597–1603.
- Yang, J., Li, Y., Feng, J., Hu, J., Liu, A., 2017. Simulation and experimental research on trans-media vehicle water-entry motion characteristics at low speed. *PloS One* 12 (5).
- Yan, G.X., Pan, G., Shi, Y., Chao, L.M., Zhang, D., 2018. Experimental and numerical investigation of water impact on air-launched AUVs. *Ocean Eng.* 167, 156–168.
- Zhang, G., Wang, S., Sui, Z., Sun, L., Zhang, Z., Zong, Z., 2019. Coupling of SPH with smoothed point interpolation method for violent fluid-structure interaction problems. *Eng. Anal. Bound. Elem.* 103, 1–10.
- Zeraatgar, H., Malekmohammadi, J., Javaherian, M.J., Moradi, H., 2019. Sampling rate effect on wedge pressure record in water entry by experiment. *Ocean Eng.* 179, 51–58.